Eindhoven University of Technology

Department Applied Physics
Plasma Physics and Radiation Technology
Coherence and Quantum Technology

Simulating the Hydrogen Molecule and Quantum Magnetism using a Variational Quantum Eigensolver

Bachelor Thesis

Supervisor: S.J.J.M.F. Kokkelmans
Author: J.J. Postema
0940055

Abstract

Quantum computing is a promising tool for understanding chemistry and physics. A universal quantum computer that prepares hundreds of qubits for a circuit utilizing on the order of 10^5 gate operations is expected to show quantum supremacy in various computational fields. The simulation of quantum systems, such as nuclear fusion, molecular bonding and chemical reactions, may be one of the very first examples where quantum supremacy emerges due to the employment of a small number of qubits and gate operations. In this thesis, a hybrid computer utilizing the advantages of both classical and quantum computing is presented. The core algorithm of this computer, which exploits the variational principle and optimization techniques to find the ground energy of quantum systems, is elaborated on, as well as a formalism for the translation of physical and chemical problems to the language of qubits and quantum circuits. These algorithms are applied to the calculation of the bonding potential curve of the hydrogen molecule and to find the spin configurations for an anti-ferromagnetic 4-particle spin-lattice.

Contents

1 Introduction

Classical computation is based on a clever arrangement of transistors, whose number grows exponentially over time according to Moore's Law. By continuously scaling down transistors, more fit inside an integrated circuit, thereby increasing the circuit's computational power. But this process is about to hit its physical limits. When the size of a transistor becomes of the order of the wavelength of the electrons that make up the electrical current, quantum effects start dominating the process of switching electronic signals. A computer that fully works on the principles of quantum mechanics can effectively evade this problem.

No universal quantum computer exists yet, but little quantum registers that are optimized for a certain problem do. It is yet unsure whether full quantum supremacy can be achieved using quantum computation, but several problems such as factoring integers and finding a number in a random array have been shown to be more effectively solved by quantum algorithms [1][2]. The full potential of quantum computers is expected to be unlocked beyond the order of $10^2 - 10^3$ qubits. The dimension of the Hilbert space $\mathcal{B}$ that describes a quantum system grows exponentially with its entries [3]. Merely 10 qubits can already probe the Hilbert space that is described by 2^{10} bits. This gives quantum computation a serious advantage over classical computation.

A hybrid computer is envisioned in which the computation-efficient properties of both the classical computer and the quantum register are combined such that it is granted superiority over existing computers. The quantum register is efficient at performing real-time simulations, whereas the classical computer is efficient at running optimization processes and arithmetic operations. This combination of both worlds leads to a computer with at its core a small quantum co-processor that can solve classically intractable problems. The simulation of quantum systems on such a computer may be one of the very first successes in the field of quantum computing as only a few amount of qubits and gate operations is needed for the computation. It is promising in the fields of chemistry, physics and computer science. Instead of the straight calculation of physical properties on a classical computer, a quantum computer allows for the real simulation of quantum systems by actual quantum systems. To illustrate this with an example, this technique can be used to find the potential curve of molecular bonding. Physical quantities that are important in determining the chemical properties of said molecule, such as the bonding energy, can be extracted from this curve.

Older methods include the PEA (Phase Estimation Algorithm), an algorithm which lets the circuit input evolve over time according to the unitary $U = \exp(-i\mathcal{H}t)$, where $\mathcal{H}$ is the Hamiltonian describing the system and t is the time [2][4]. For sufficiently long evolutions, the Fourier spectrum can be resolved. Running the phase estimation algorithm over the system gives the eigenenergy of the system. Recently, a new algorithm has been put forward that does not depend on time evolutions: the variational quantum eigensolver [5][6]. This algorithm parameterizes a trial wave function and approximates its energy by sampling the Pauli terms that make up a system's Hamiltonian. A gradient descent algorithm can update the variational parameters to minimize the energy, eventually converging towards the ground energy of the system. The latter method will be the core technology of the proposed hybrid computer.

In section 2, the theory of the variational quantum eigensolving algorithm is explored. Section 3 discusses the application to simulating the hydrogen molecule. Additionally, in section 4, the algorithm is applied to simulating quantum magnetism. A conclusion and a small outlook on the future is given at the end in section 5.

2 Variational quantum eigensolving

2.1 The variational principle

The variational principle is a principle in quantum mechanics that states that for a given Hamiltonian $\mathcal{H}$ and any wave function $|\Psi\rangle$ chosen at random, the Hamiltonian eigenvalue of said wave function will always be equal to or an overestimation of the actual ground eigenenergy E_G of $\mathcal{H}$. Therefore, for any not necessarily normalized $|\Psi\rangle$, the inequality

$$\langle \mathcal{H} \rangle_{|\Psi\rangle} \stackrel{\text{def}}{=} \frac{\langle \Psi | \mathcal{H} | \Psi \rangle}{\langle \Psi | \Psi \rangle} \geq E_G \tag{2.1}$$

holds.

Let a given quantum system be described by individual two-level quantum systems, each described by a point on the Bloch sphere. The entire configuration can be parameterized by a set of coefficients, called the variational parameters. In the case of qubits, the parameters could signify the azimuthal (θ) and polar (φ) angles of the system's location on the Bloch sphere, as depicted in figure 2.1. For a given Hamiltonian that has a distinct energy minimum, there must exist a set of parameters such that the energy function $\langle \mathcal{H} \rangle_{|\Psi\rangle}$ is minimized. This principle can be applied to what is known as the variational quantum eigensolving algorithm.

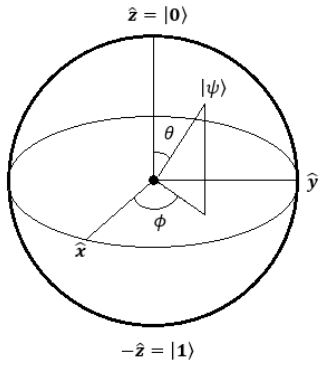

Figure 2.1: The Bloch sphere, where the states $|0\rangle$ and $|1\rangle$ are assigned to the north and south pole respectively.

2.2 The VQE algorithm

2.2.1 General overview

The variational quantum eigensolving (VQE) algorithm is an algorithm that finds the set of parameters for which the eigenvalue of an operator is minimized. If said operator is a Hamiltonian that describes a quantum system, the physical meaning of this minimal eigenvalue is the ground energy of the system.

The algorithm can be divided into 5 parts [7]:

1. The Hamiltonian of the quantum system that is to be simulated is transformed into a series of Pauli operators. These terms are generated by the Jordan-Wigner transformation (see section 3.2) or the system's properties (see section 4.1). If possible, the amount of qubits is reduced. This will be further discussed in section 3.3.
2. A quantum circuit prepares a state that is parameterized by a set $\vec{\theta}$ containing all parameters that

specify the rotations around the Bloch spheres of the individual qubits. If the vacuum state[1] $|0...0\rangle$ is taken to be the input of the state preparation circuit, the associated Hilbert space can be probed by sufficient parameterization. This means that any part of the Hilbert space must be accessible for some set of parameters to make sure any minimum can be found. If necessary, depth can be added to the circuit by alternating Bloch sphere rotations with entanglement operations, to be explained in section 2.2.3.

3. The energy of the prepared state is measured in the neighbourhood of $\vec{\theta}$ by sampling the individual Pauli terms that make up the Hamiltonian. The classical computer performs arithmetic operations to calculate this energy.
4. The measured energy values are sent to a classical optimization algorithm that prepares a new set of parameters such that in the long run a better approximation to the actual ground energy is acquired.
5. This process repeats itself for either a user-specified amount of iterations or until the algorithm has reached convergence within a desired accuracy. In chemistry, chemical accuracy is the desired accuracy that is aimed for, corresponding to an absolute error of 0.043 eV [8].

2.2.2 Rotational quantum gates

Any unitary single-qubit operator U can be decomposed into rotations on the Bloch sphere and a phase gain, such that

$$U = e^{i\alpha} R_z(\beta) R_x(\gamma) R_z(\delta) \tag{2.2}$$

for a given set of parameters $\alpha, \beta, \gamma, \delta$ [9]. The operators $R_z(\beta)$ and $R_x(\gamma)$ denote a rotation of β radians around the z-axis on the Bloch sphere and a rotation of γ radians around the x-axis respectively. Likewise, a $R_y(\epsilon)$ rotation would describe a rotation of ϵ radians around the y-axis. These rotations are given by:

$$R_x(\epsilon) = \cos(\epsilon/2)\mathbb{1} + i\sin(\epsilon/2)X \stackrel{\text{def}}{=} X_\epsilon, \tag{2.3}$$

$$R_y(\epsilon) = \cos(\epsilon/2)\mathbb{1} + i\sin(\epsilon/2)Y \stackrel{\text{def}}{=} Y_\epsilon, \tag{2.4}$$

$$R_z(\epsilon) = \cos(\epsilon/2)\mathbb{1} + i\sin(\epsilon/2)Z \stackrel{\text{def}}{=} Z_\epsilon. \tag{2.5}$$

Here, $\mathbb{1}$ represents the identity operator and X, Y and Z are the Pauli spin matrices σ^x,σ^y and σ^z. They are given by

$$\mathbb{1} = \begin{pmatrix} 1 & 0 \\ 0 & 1 \end{pmatrix}, X = \begin{pmatrix} 0 & 1 \\ 1 & 0 \end{pmatrix}, Y = \begin{pmatrix} 0 & -i \\ i & 0 \end{pmatrix}, Z = \begin{pmatrix} 1 & 0 \\ 0 & -1 \end{pmatrix}. \tag{2.6}$$

For the rest of this thesis, $\mathbb{1}$ is referred to as a Pauli operator.

2.2.3 The circuit

The identity (2.2), or ZXZ-rotation in short, can be exploited for quantum computing. Any arbitrarily chosen point on the Bloch sphere can be reached by such a series of rotations, where for simplicity, α is chosen to be 0. Once parameterized, it is written as

$$\mathcal{U}_{q,i}(\vec{\theta}) = Z_{\theta_1^{q,i}} X_{\theta_2^{q,i}} Z_{\theta_3^{q,i}}. \tag{2.7}$$

Here, q identifies the qubit on which the operator is acting, i refers to the depth in which the operators are nestled and the $\theta_m^{q,i}$ coefficients are the variational parameters.

[1] The word 'vacuum' is merely a convention and does not always physically correspond to an empty state despite its insinuation.

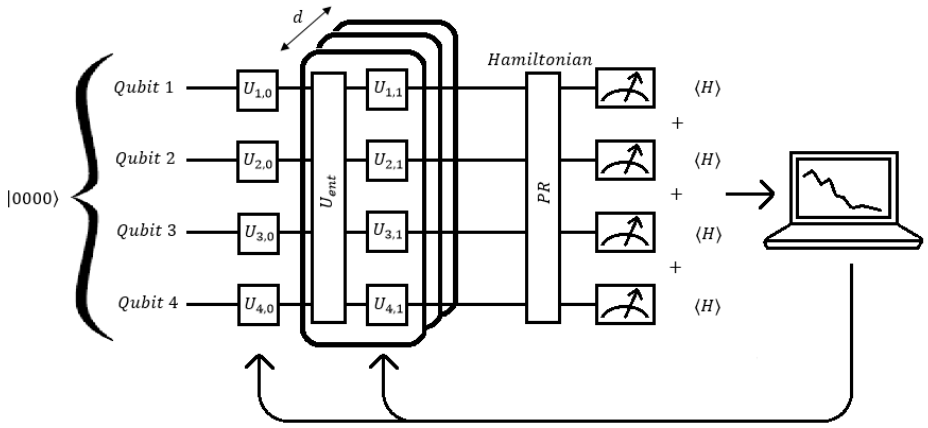

Figure 2.2: The VQE circuit for 4 qubits. The rectangular block $\mathcal{U}_{ent}$ refers to the multi-qubit entanglement operation and the PR block refers to the single-qubit post-rotations that are applied before measurement. d signifies the depth of the system; every additional degree of depth introduces another entanglement operation and a new set of ZXZ-rotations $\mathcal{U}_{q,d}$. Addition is performed on a classical computer that also runs the SPSA algorithm. A feedback loop is added to update the parameters.

The trial state is parameterized using two types of unitary operators: rotation gates $\mathcal{U}_{q,i}(\vec{\theta})$ and entanglement operators $\mathcal{U}_{ent}$[2]. A vacuum state is taken to be the input such that the final trial state for a d-depth circuit utilizing N qubits equals

$$|\Psi(\vec{\theta})\rangle = \prod_{q=1}^{N}(\mathcal{U}_{q,d}(\vec{\theta})) \times \mathcal{U}_{ent} \times \prod_{q=1}^{N}(\mathcal{U}_{q,d-1}(\vec{\theta})) \times \mathcal{U}_{ent} \times \cdots \times \mathcal{U}_{ent} \times \prod_{q=1}^{N}(\mathcal{U}_{q,0}(\vec{\theta}))\,|00\cdots00\rangle\,. \tag{2.8}$$

The input of the system is the set of the north poles of the N Bloch spheres describing the system. No rotation around the Z-axis can alter this state, thus the first Z-rotations are omitted. The variational parameters that are associated with the resulting rotations induce a parameter space P that the gradient descent algorithm probes. Its dimension is given by

$$\dim(P) = (2+3d)N \stackrel{\text{def}}{=} p. \tag{2.9}$$

The entire circuit is shown in figure 2.2 for the specific case of 4 qubits. In general, one may design a circuit for any arbitrary amount of qubits by downwards extension of the circuit.

2.2.4 Measurement

The Hamiltonian of the system that is to be simulated must be incorporated into the system. This does not happen directly, though. First, the Hamiltonian must be mapped to sums of tensor products of Pauli operators. In section 3.2, a reliable mapping is introduced for molecular structures in the field of quantum chemistry and in section 4.1, the Hamiltonian of a quantum magnet is given, which finds itself only in the formalism of Pauli terms. Such transformed Hamiltonians, working on N qubits, take the form

$$\mathcal{H} = \sum_{\substack{a_1,a_2,\cdots,a_N \\ 1\le a_i\le 4}} h_{a_1,a_2,\cdots,a_N} P_{a_1} \otimes P_{a_2} \otimes \cdots \otimes P_{a_N} \stackrel{\text{def}}{=} \sum_{\substack{a_1,a_2,\cdots,a_N \\ 1\le a_i\le 4}} h_{a_1,a_2,\cdots,a_N} P_{a_1} P_{a_2} \cdots P_{a_N}. \tag{2.10}$$

Here, $h_{a_1,a_2,\cdots,a_N}$ denote real coeffients that can be precomputed classically. The subscript numbers of the a-coefficients indicated the qubit on which the operator is acting. The values of the a-subscripts

[2]There are no hard constraints on this operator as long as sufficient entanglement is achieved. The entanglement phase directly impacts the accuracy of the measurements, though, and chemical accuracy is only achieved for a certain entanglement phase. Computer simulations don't have to take this effect into account, however, if no error and fluctuations are imposed on the system.

indicate the desired Pauli operator according to the identification $\{P_1, P_2, P_3, P_4\} \to \{\mathbb{1}, X, Y, Z\}$. To take an example, if $\{a\} = \{1, 3, 4, 2\}$, then $P_{a_1} \otimes P_{a_2} \otimes P_{a_3} \otimes P_{a_4} = \mathbb{1} \otimes Y \otimes Z \otimes X$.

A quantum register is not able to directly measure the Hamiltonian. It is, however, able to sample all the constituent parts that make up the Hamiltonian. By linearity, the expectation value $\langle \mathcal{H} \rangle$ may be constructed by superposition of the individually sampled terms according to

$$\langle \mathcal{H} \rangle = \sum_{\substack{a_1, a_2, \cdots, a_N \\ 1 \leq a_i \leq 4}} h_{a_1, a_2, \cdots, a_N} \langle P_{a_1} P_{a_2} \cdots P_{a_N} \rangle . \tag{2.11}$$

It becomes clear that the Hamiltonian does not have to be integrated into the circuit directly if the geometrical properties of the Bloch sphere are considered. By definition, a measurement takes place in the Z-basis. A measurement of the expectation values of other Pauli operators, $\langle \mathbb{1} \rangle, \langle X \rangle$ or $\langle Y \rangle$, relies on a post-rotation that is applied to the prepared trial state (2.8). After a $-\frac{\pi}{2}$-rotation around the Y-axis, the X-axis has now replaced the old Z-axis. Measurement therefore yields the result for $\langle X \rangle$. Similarly, measuring a qubit after a $\frac{\pi}{2}$-rotation around the X-axis yields a $\langle Y \rangle$-measurement.

For other (composite) Pauli terms, a slightly different approach is required. In Appendix A, a measurement protocol is elaborated on that explains how any Pauli tensor product can be sampled on the quantum circuit given in figure 2.2.

2.3 The SPSA gradient descent

The simultaneous perturbation stochastic approximation (SPSA) is a gradient descent algorithm that takes as an input a set of variables $\vec{\theta}$, that parameterizes an objective function, and updates these variables in an iterative process such that the function value will on average decrease. Under certain circumstances, the algorithm guarantees convergence towards the global/local minimum even under the influence of stochastic perturbations. The location of $\vec{\theta}$ in the p-dimensional parameter space is most important in determining towards which minimum the algorithm guarantees convergence. For a given wave function $|\Psi(\vec{\theta})\rangle$, the algorithm can find the ground energy of a system that is described by the Hamiltonian $\mathcal{H}$. This is guaranteed since the ground energy is the minimum of the objective function $\langle \Psi(\vec{\theta}) | \mathcal{H} | \Psi(\vec{\theta}) \rangle$.

To descend opposite of the gradient, the algorithm evaluates the energy at two different locations, regardless of the value of p [10]. For every iteration k, the two values $\vec{\theta}_{k,\pm} = \vec{\theta}_k \pm c_k \vec{\Delta}_k$ are sampled. Here, c_k denotes a constant that depends on the iteration step k and $\vec{\Delta}_k$ is a p-dimensional vector that is randomly generated by any randomizer that is sufficiently random. Here, its entries are determined by the Rademacher distribution, such that each slot in the vector has a 50% chance to be occupied by a 1 and a 50% chance to be occupied by a -1.

The gradient $\vec{g}_k$ is approximated as follows:

$$\vec{g}_k = \frac{\langle \Psi(\vec{\theta}_{k,+}) | \mathcal{H} | \Psi(\vec{\theta}_{k,+}) \rangle - \langle \Psi(\vec{\theta}_{k,-}) | \mathcal{H} | \Psi(\vec{\theta}_{k,-}) \rangle}{2c_k} \vec{\Delta}_k. \tag{2.12}$$

In order to minimize the objective function value, the parameters must be updated by moving anti-parallel to the gradient in parameter space, according to

$$\vec{\theta}_{k+1} = \vec{\theta}_k - a_k \vec{g}_k, \tag{2.13}$$

where a_k is a weight factor that is also dependent on the iteration step k. Both a_k and c_k are of the same form:

$$a_k = \frac{a}{k^A}, \tag{2.14}$$

$$c_k = \frac{c}{k^\Gamma}. \tag{2.15}$$

The constants A and Γ are best chosen to be 0.602 and 0.101 to guarantee that the smoothest gradient descent possible through parameter space takes place [11]. Earlier simulations have shown that the constant c is optimally taken to be 0.1. a is a parameter that depends on measurements and is calibrated

such that a reasonable angle update is guaranteed for the first iteration steps. This is realized by taking

$$a = \frac{2\pi}{5} \frac{c}{\langle | \langle \Psi(\vec{\theta}_{1,+})|\mathcal{H}|\Psi(\vec{\theta}_{1,+})\rangle - \langle \Psi(\vec{\theta}_{1,-})|\mathcal{H}|\Psi(\vec{\theta}_{1,-})\rangle | \rangle_{\vec{\Delta}_1}}, \tag{2.16}$$

where the denominator signifies an average over multiple samples that are generated by the vector $\vec{\Delta}_1$.

3 Simulating quantum chemistry

3.1 Molecular Hamiltonians

The electronic configuration of an atom or molecule is characterized by the spin-orbitals of the individual electrons. Spin-orbitals are a generalization of atomic orbitals in which the spin of the electron is accounted for. Let ϕ_i denote the i-th electron spatial wave function and let S_i denote the spin function of that electron. The spin-orbital is then given by $\chi_i = \phi_i S_i$ and is parameterized by σ, which is shorthand for the vector (x, ω), where x denotes the three spatial coordinates and ω denotes an abstract spin variable.

The abstractly defined spin functions, $\alpha(\omega)$ and $\beta(\omega)$, are the spatial equivalent of respectively the state vectors $|\uparrow\rangle$ and $|\downarrow\rangle$, analogous to how the spatial wave function ψ is equivalent to the projection $\langle x|\psi\rangle$ of the state vector $|\psi\rangle$. These spin functions satisfy the orthogonality principles

$$\int \alpha^*(\omega)\alpha(\omega)\, d\omega = 1, \tag{3.1}$$

$$\int \beta^*(\omega)\beta(\omega)\, d\omega = 1, \tag{3.2}$$

$$\int \alpha^*(\omega)\beta(\omega)\, d\omega = 0, \tag{3.3}$$

$$\int \beta^*(\omega)\alpha(\omega)\, d\omega = 0. \tag{3.4}$$

Let M denote the total amount of spin-orbitals in a molecule and let $\mathcal{B}$ denote the Hilbert space of such a spin-orbital. The associated Hilbert space of a given electronic Hamiltonian is then given by $\mathcal{B}^{\otimes M}$. A neutral molecule contains $\frac{M}{2}$ electrons, if no excited orbitals are considered and no pairs of electrons with opposite spin occupy the same atomic orbital, and therefore only a part of the associated Hilbert space is probed. This allows for a reduction scheme in qubits, presented in subsection (3.3).

There are two ways to tackle an electronic structure problem: the first and second quantization methods. In the former method, spatial wave functions and their correlation integrals are considered, called the Hartree-Fock method. In the latter method, the system is treated using fermionic field operators and Fock states, originating from quantum field theory. The first quantization treatment for the hydrogen molecule can be found in Appendix B and as it turns out, this will be fully equivalent to the second quantization method, which will be discussed later on in this section.

Under the Born-Oppenheimer approximation, the second quantized Hamiltonian of the electrons in their orbitals in a molecule is given by the general expression [12]

$$\mathcal{H} = \sum_{p,q=1}^{M} h_{pq} a_p^\dagger a_q + \frac{1}{2} \sum_{p,q,r,s=1}^{M} h_{pqrs} a_p^\dagger a_q^\dagger a_r a_s. \tag{3.5}$$

In this expression, the h_{pq} and h_{pqrs} terms are molecular integrals that can be precomputed classically. The $a_p^\dagger(a_p)$ operators are the creation (and annihilation) operators that work on local fermionic mode p. These operators induce the fermionic algebra $\mathcal{F}$ of the anti-commutation relationships

$$\{a_i, a_j\} = 0, \tag{3.6}$$

$$\{a_i^\dagger, a_j^\dagger\} = 0, \tag{3.7}$$

$$\{a_i, a_j^\dagger\} = \delta_{ij} \tag{3.8}$$

on the associated Hilbert space [13].

The molecular integrals are defined on basis of the spin-orbitals and are given by [12]

$$h_{pq} = \int \chi_p^*(\sigma)(-\frac{\nabla^2}{2} - \sum_i \frac{Z_i}{\rho_i})\chi_q(\sigma)\, d\sigma, \tag{3.9}$$

$$h_{pqrs} = \iint \frac{\chi_p^*(\sigma_1)\chi_q^*(\sigma_2)\chi_r(\sigma_2)\chi_s(\sigma_1)}{|r_1 - r_2|}\, d\sigma_1\, d\sigma_2 \tag{3.10}$$

in Hartree atomic units[3]. Z_i is the nuclear charge of the i-th nucleus, ρ_i is the distance between nucleus i and an electron in spin-orbital $\chi_q(\sigma)$ and $|r_1 - r_2|$ is the distance between electron 1 and 2. Furthermore, $d\sigma$ is shorthand for the elementary volume measure $dV d\omega$, where dV is an infinitesimally small volume element.

These definitions assign a clear role to each component in the Hamiltonian (3.5). The first term describes the kinetic and potential energy of the electrons in an orbital around the nuclei, while the second term describes the Coulombic electron repulsion. The nature of the Born-Oppenheimer approximation emerges here: the integrals (3.9) and (3.10) do not involve the electrostatic repulsion of the nuclei, nor do they involve their kinetic energies.

3.2 The Jordan-Wigner transformation

For experimental purposes, qubits must be distinguishable entities. Electrons, however, are fermions and therefore indistinguishable. A reliable mapping from fermionic operators to quantum gates can circumvent this problem. The Jordan-Wigner transformation is an example of such a mapping. It expresses fermionic operators as tensor products of the identity operator $\mathbb{1}$ and the other Pauli operators X, Y and Z that correspond to the algebra of spin-$\frac{1}{2}$ particles. Other mappings such as the Bravyi-Kitaev transformation exist, but they are invoked less in literature than the Jordan-Wigner transformation.

The Jordan-Wigner transformation is given by

$$a_j = \mathbb{1}^{\otimes j-1} \otimes \sigma^+ \otimes Z^{\otimes N-j}, \tag{3.11}$$

$$a_j^\dagger = \mathbb{1}^{\otimes j-1} \otimes \sigma^- \otimes Z^{\otimes N-j}, \tag{3.12}$$

where N is the total amount of qubits that is required for the simulation. The new operators $\sigma^\pm$ are given by

$$\sigma^\pm = \frac{X \pm iY}{2}. \tag{3.13}$$

The molecular Hamiltonian describing a molecule can now be transformed into a set of Pauli operations. A small quantum register can simulate this efficiently.

3.3 Tapering off qubits

In second quantization form, electronic Hamiltonians such as (3.5) possess a block diagonal structure. Each block corresponds to a certain amount of electrons in the system. For neutral molecules with electrons in their lowest energetic non-spin-degenerate orbitals, there are $\frac{M}{2}$ electrons, which leaves the Hamiltonian matrix with a lot of entries that neither interact with the right block corresponding to $\frac{M}{2}$ electrons nor have any functionality on their own in the discussion of neutral molecules.

The general strategy is to filter out blocks that do not correspond to the right amount of electrons, whatever its value is between 0 and M. This leaves a sparse matrix behind, out of which a lot of rows and columns can be removed. By shifting columns and rows, one can taper off 2 qubits in the process.

Let the general Hamiltonian of an electronic system be given by $\mathcal{H}^M$, where the superscript M represents the amount of spin-orbitals. A projection can reduce this matrix to one containing only the block that describes N electrons. The projector operator is given by

$$\Pi_N^K = \prod_{j \neq N}^{K} \frac{N_T - j}{N - j}, \tag{3.14}$$

[3]Hartree atomic units take the following constants to be equal to 1: the electron mass m_e, the elementary charge e, Coulomb's constant $\frac{1}{4\pi\epsilon_0}$ and Planck's reduced constant $\hbar$. The resulting energy is in Hartree units, where 1 Hartree is equal to ~ 27.2eV.

where N_T represents the total number of electrons and is given by the sum of the occupation numbers of each individual spin-orbital. The desired reduced Hamiltonian is acquired by squeezing the Hamiltonian between the projectors according to

$$\mathcal{H}_K^M = {\Pi_N^K}^\dagger \mathcal{H}^M \Pi_N^K. \tag{3.15}$$

For the rest of this subsection, the hydrogen molecule is considered. Let the 4 qubits that would be required for the Hamiltonian in (3.15) represent the following spin-orbitals: qubits 1 and 3 correspond to a spin-up and spin-down electron respectively in the first molecular orbital (bonding), while qubits 2 and 4 represent a spin-up and spin-down electron respectively in the second molecular orbital (anti-bonding). The potential landscape of the hydrogen molecule can be probed by considering the spin singlet configuration. In this case, the projector takes the form

$$\Pi_N^K = \Pi_2^4 = N_\uparrow(2 - N_\uparrow)N_\downarrow(2 - N_\downarrow). \tag{3.16}$$

Here, $N_\uparrow$ is defined as the total number of spin-up electrons and $N_\downarrow$ is defined as the total amount of spin-down electrons. One can take projector (3.16) and translate it to tensor products of Pauli matrices according to the Jordan-Wigner transformation:

$$\Pi_2^4 = \frac{1}{4}(\mathbb{1}^{\otimes 4} - Z_1\otimes Z_2\otimes \mathbb{1}^{\otimes 2} - \mathbb{1}^{\otimes 2}\otimes Z_3\otimes Z_4 + Z_1\otimes Z_2\otimes Z_3\otimes Z_4) \stackrel{\text{def}}{=} \frac{1}{4}(1 - Z_1Z_2 - Z_3Z_4 + Z_1Z_2Z_3Z_4). \tag{3.17}$$

P_i refers to the Pauli operator $P \in \{\mathbb{1}, X, Y, Z\}$ acting on qubit i. In Appendix C, a rigorous qubit reduction scheme can be found. After following this scheme, the final hydrogen Hamiltonian $\hat{\mathcal{H}}$ looks like

$$\hat{\mathcal{H}} = g_0\mathbb{1}\mathbb{1} + g_1(Z\mathbb{1} + \mathbb{1}Z) + g_2XX + g_3ZZ = \begin{pmatrix} g_0 + 2g_1 + g3 & 0 & 0 & g_2 \\ 0 & g_0 - g_3 & g_2 & 0 \\ 0 & g_2 & g_0 - g_3 & 0 \\ g_2 & 0 & 0 & g_0 - 2g_1 + g3 \end{pmatrix}, \tag{3.18}$$

in which the g-coefficients are identified in the qubit reduction process in Appendix C.

The similarities between equation (3.18) and an exact calculation as given in Appendix B are easily identified. On the diagonal, the electrostatic proton-proton repulsion is given. Likewise, this repulsion is added up as a constant in equation (A.14). The same goes for the ground energy, as in the limit of infinite separation, only one-electron terms remain, finding themselves on the diagonal. The complex overlap and exchange integrals are less easily identified, but they are implicitly found within the other g-coefficients.

3.4 Simulations of H_2

3.4.1 Methods

The potential curve for H_2 is acquired by simulating the quantum circuit, depicted in figure 2.2, on a classical computer. This is possible because of the simplicity and symmetries of the hydrogen molecule. For more complex molecules, the calculations will become exponentially harder to simulate to the point of being intractable. A real quantum computer must take over at that point and perfect classical simulations can not be relied on any more. An exact Hartree-Fock calculation is run as well for comparison.

The quantum circuit is simulated using Matlab [14]. The exact Hartree-Fock curves are calculated using Matlab as well [15][16]. Quantum computation at the fundamental level boils down to matrix multiplication, which Matlab is excellent at. For both simulations, the STO-3G basis is employed for the calculations of the interaction integrals. No decoherence and gate deficiencies are imposed on the system and no external perturbations or stochastic fluctuations are present. Henceforth, this shall be referred to as a 'perfect simulation'.

For the perfect simulations of the hydrogen molecule, a 2-qubit system is prepared, in agreement with section 3.3. A depth $d = 1$ has been opted for, as real simulations have shown that this depth is the critical depth for the simulation the hydrogen molecule [6]. For the unchanged Hamiltonian (see (A.16) in

Appendix C), the 4 qubits can be mapped one-to-one to the four spin-orbitals of the hydrogen molecule. The 2 remaining qubits after the matrix reduction represent the ground state and the excited states of the singlet configuration [17]. The influence of depth on the accuracy of the simulations is not as tough as its influence on real simulations due to the lack of fluctuations in a perfect simulation. In section 4.1, it is shown that for some systems depth can have a notable influence on the final results.

3.4.2 Potential curves

Using the VQE algorithm and the two-qubit hydrogen molecule Hamiltonian that had been built in section (3.3), simulations have been run to plot the potential curve of two hydrogen atoms as they would approach each other as function of their distance R. They are shown in figure 3.1. The values for the g-coefficients that make up the Hamiltonian can be found in Appendix D.

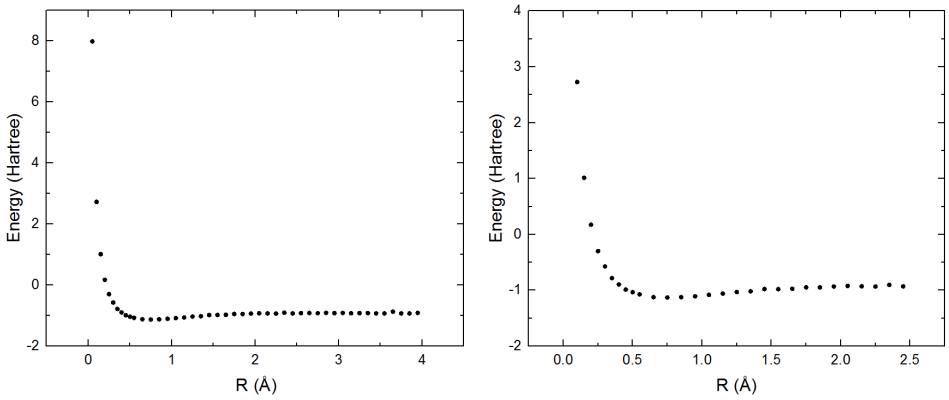

(a) The H_2 potential landscape.

(b) The H_2 potential landscape zoomed in.

Figure 3.1: The potential landscape of H_2, as calculated by the VQE algorithm as function of the inter-nuclear distance R. Two different scales have been chosen.

As expected, a clear bonding state can be distinguished at $R \approx 0.75$Å, compared to the experimental value of 0.7414 Å [18]. The behaviour that this plot shows is in agreement with experiments and theory. For short inter-nuclear distances, the enormous nuclear repulsion will render the configuration unstable. For long inter-nuclear distances, there is hardly any orbital overlap, causing a tiny attractive force to emerge. For intermediate distances around the equilibrium distance, there is a slight dip in the curve that signifies that a bonding state exists.

To gauge the accuracy of these results, the simulation data are laid over the exact Hartree-Fock curve in figure 3.2.

At first sight, the simulation data points seem to look like a near carbon-copy of the data points that make up the exact curve, as picture 3.2.(a) may suggest. Upon closer inspection, however, there seem to be discrepancies when moving further from the equilibrium bonding length in both directions. These errors can be explained from a physical point and view and will be discussed in the next section.

3.4.3 A word on convergence

The nature of the SPSA algorithm is best visualized by comparing different plots for different iteration lengths. In figure 3.3, a comparison is made for plots that ran on simulations using 1, 10 and 100 iteration steps. As the path through parameter space is random, it is possible that following the gradient will always lead to an increase in the energy, no matter what direction along the gradient one moves along. This can also be seen in the figure: on average, the algorithm outputs a better approximation of the exact Hartree-Fock energy, but on small iteration scales, the energy may increase. At some distances, the

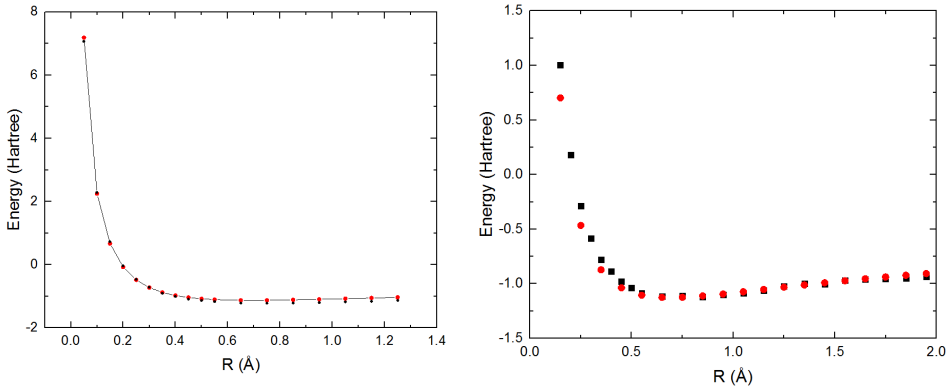

(a) (b)

Figure 3.2: Comparison of the simulated potential curve (black squares) and the exact Hartree-Fock potential (red circles and line) as function of the inter-nuclear distance R.

estimated energy after 10 iterations is even worse than after a single iteration. This effect will on average diminishes during the iteration process.

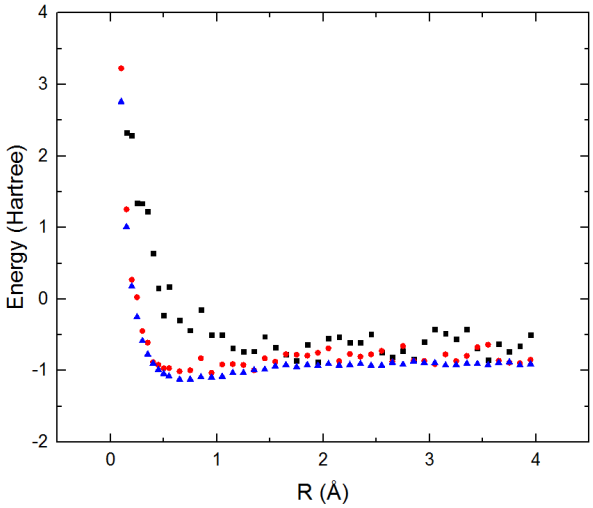

Figure 3.3: The convergence of the energy for 1 (black squares), 10 (red circles) and 100 (blue triangles) iteration steps as a function of the inter-nuclear distance R.

One may also compare the absolute and relative errors during this convergence process. These errors are given in figure 3.4.

For longer iterations, the absolute values of both the absolute and relative errors decrease. This is expected as the answer should be more accurate for longer paths through parameter space. For shorter inter-nuclear distances, the absolute error is high compared to longer distances. This can be explained by the high gradient caused by the proton-proton repulsion. At very short distances, this electrostatic repulsion dominates the potential curve with a very sharp gradient. A small error in the Hamiltonian coefficients may therefore cause a large error in the final answer. For longer bonding lengths, the gradient is not sharp any more and small errors remain small on average. For 100 iterations, the absolute error for long distances R is on the order of 0.1 eV. This is appreciable, but it does not fall within the chemical accuracy regime. The relative error, on the other hand, is pretty constant over all distances R, apart from a divergence around $R = 0.2$ Å where the energy approaches 0. This again shows that there is nothing special about the high absolute error at low distances: it is merely an artifact of the steep gradient.

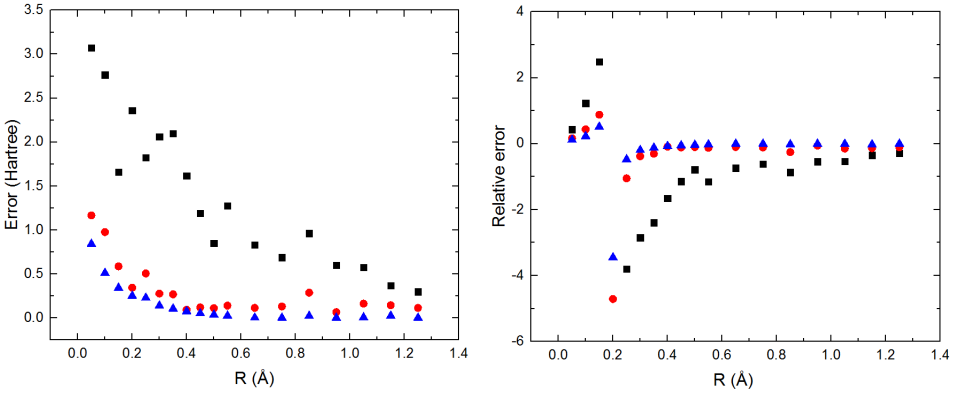

(a) The absolute error.

(b) The relative error. One data point at R =0.2Å has been left out for the sake of compactness of the image.

Figure 3.4: The errors between the Hartree-Fock curve and the simulation for 1 (black squares), 10 (red circles) and 100 (blue triangles) iteration steps as a function of the inter-nuclear distance R.

3.5 Generalization for other molecules

The method that has been used in this section can be generalized to other molecules. H_2 is the simplest molecule that exists; it encompasses a linear geometry and the electrons are in their ground state $1s$ orbitals. The simulation becomes challenging when the respective molecule is not linear any more. Even in this category, multiple classes of complexity may be distinguished. The water molecule H_2O is easier to simulate, for instance, than a benzene ring or ethanol, where additional advanced mathematics is required for the computation.

The geometry of a problem is implicitly taken as an input. The integrals are dependent on spatial wave functions that are themselves dependent on user-defined coordinates. In general, it is not difficult to include the geometry in the problem, but it makes the algorithm run longer. Computational strain may arise, however, if the geometry of the system permits complex overlap of the orbitals.

Tapering off qubits is a process that is not restricted to the hydrogen molecule only. It has been shown that one can taper off qubits for the Fermi-Hubbard system [19] and for LiH and BeH_2 molecules [6][11]. In the latter case, 2 qubits may be taken off for both molecules. The difference between simulating hydrogen and slightly more complex molecules arises upon consideration of the inner electron shells. For molecules with constituent atoms close to hydrogen on the periodic table, the $1s$ shells may be assumed to be filled. This leads to the concept of dressed states, which has not been discussed in this thesis. The Bogoliubov transformation is an important tool for the calculation of the potential curves of these more complex molecules [11]. This is beyond the scope of this thesis, however, but it illustrates well that there is more pre-computational consideration necessary than for the hydrogen molecule.

It remains a difficult problem to simulate more complex molecules on a quantum register. Future research will likely bring more techniques to tackle such issues.

4 Simulating quantum magnetism

4.1 The Heisenberg model

The Heisenberg model is a quantum mechanical model that describes particles in a lattice that interact with one another through spin-spin coupling in the presence of an external magnetic field, mostly used for spin-$\frac{1}{2}$ particles. It serves as an extension to the Ising model, which assumes the spin of a particle is either in a spin-up ($|0\rangle$) or spin-down ($|1\rangle$) state, occupying only the poles of the Bloch sphere. The Heisenberg model, on the other hand, allows for the spins to be aligned in any direction such that they can be described by any spinor χ as an unrestricted point on the Bloch sphere.

Mapping the spins to qubits is therefore fairly natural as the components of the spinor of a single spin can be mapped one-to-one onto their respective qubit states.

The Hamiltonian of the Heisenberg model is equal to

$$\mathcal{H} = J \sum_{|\langle i,j \rangle|} X_i X_j + Y_i Y_j + Z_i Z_j - B \sum_k Z_k, \tag{4.1}$$

where J represents the coupling strength of the spin-spin interactions and B is the magnetic field strength. The first summation runs over all ordered pairs of nearest neighbours. The X, Y and Z operators are the familiar Pauli spin matrices given by equation (2.6).

Interactions that are present in a quantum magnet can be split in two parts and are captured well by the Hamiltonian (4.1). The first term in the Hamiltonian represents the spin-spin interactions between the nearest neighbours. Such interactions are defined by a strength J and inner products of spins $\vec{S}_i \cdot \vec{S}_j \equiv X_i X_j + Y_i Y_j + Z_i Z_j$. The second term in the Hamiltonian describes the tendency of the spins to align with an externally applied magnetic field. The inner product of the spin and the magnetic field determines the energy: if this product takes a larger value, the particle will have a lower energy.

An anti-ferromagnetic quantum magnet is of most interest. The spin-spin interactions cause the spins to be anti-parallel, while the external magnetic field forces the spins to be aligned along the field lines in the positive z-direction. This leads to interesting dynamics and phase transitions.

4.2 Simulations

4.2.1 Methods

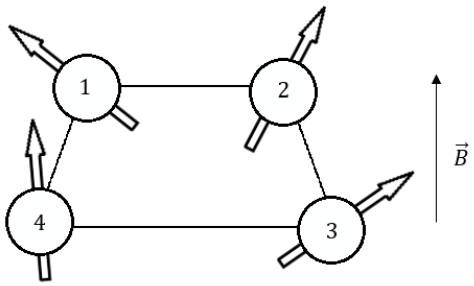

Figure 4.1: An anti-ferromagnetic square lattice under the influence of nearest-neighbour spin-spin coupling and an external magnetic field.

For this simulation, a square lattice with a spin-$\frac{1}{2}$ particle at each corner has been chosen. The system is characterized by an anti-ferromagnetic interaction term in which the value of J is positive. An external magnetic field pointing in the positive z-direction is applied to the lattice, as shown in figure

4.1. As the first summation in (4.1) implies, only the ordered sets $\{1,2\}$, $\{2,3\}$, $\{3,4\}$ and $\{1,4\}$ interact anti-ferromagnetically.

As before, the system is simulated using Matlab [14]. A zero-depth circuit is used for the simulation. The spinor χ that describes each spin on the lattice is directly mapped to qubits via

$$\chi = \begin{bmatrix} a \\ b \end{bmatrix} \rightarrow \begin{bmatrix} a \\ b \end{bmatrix} \stackrel{\text{def}}{=} a\,|0\rangle + b\,|1\rangle = |q\rangle\,. \tag{4.2}$$

Four qubits have thus been prepared for the input state, each corresponding to the spinor of their respectively particle.

4.2.2 Anti-ferromagnetic energies

For a range of values for the interaction ratio J/B, the energy is measured and is given in figure 4.2.

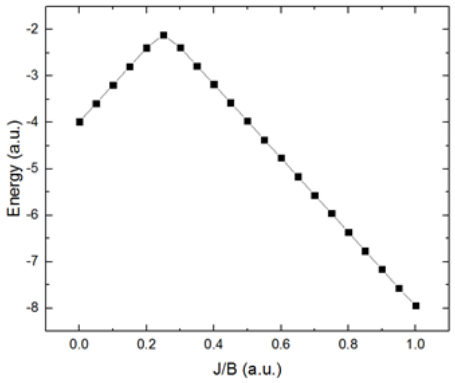

(a) A perfect simulation of the energy curve.

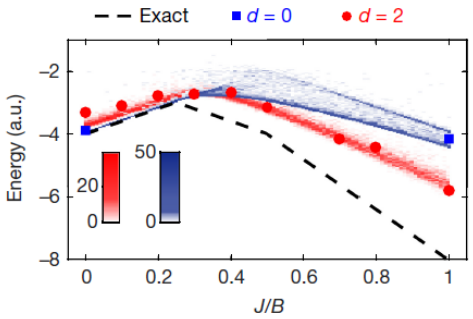

(b) The exact energy curve and two real simulations for a zero-depth and two-depth circuit [6]. The shading indicates a spread in the answers.

Figure 4.2: The energy of the spin lattice as a function of the interaction ratio J/B for perfect simulations, real simulations and an exact solution.

The perfect simulation predicts the exact energy for the regime of $J/B = 0.4{-}1.0$. As it turns out, the regime of $J/B = 0.0{-}0.4$ has a lower energy than the perfect simulation predicts, but the general shape is maintained. This can be explained by the lack of depth of the circuit. Real simulations show that a better convergence to the theoretical curve occurs for higher depth circuits. The zero-depth circuit predicts a maximum of -2, as expected, while the two-depth circuit wraps tightly around the theoretical maximum of -3. The discrepancies between the results from real simulations and the theoretical values are one of the reasons why quantum computers are hard to develop. Real quantum systems are fragile and sensitive. External perturbations, deficiencies and imperfections will lead to a result that is off from theoretical predictions.

Apparently, the magnet's energy is lowest for entangled states between $J/B = 0.0{-}0.4$. Sufficient entanglement could not be achieved with a zero-depth circuit and no kink can be observed in the energy plot 4.2(a).

4.2.3 A word on convergence

This example of anti-ferromagnetism on the quantum scale is a good showcase of the properties of the SPSA algorithm.

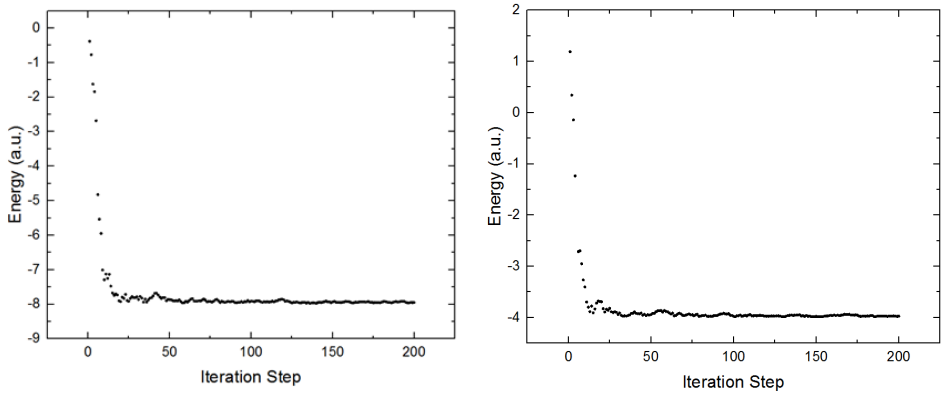

(a) Convergence towards the state $|0101\rangle$ or a rotational variant of it.

(b) Convergence towards the state $|0110\rangle$ or a rotational variant of it.

Figure 4.3: The energy of the spin lattice as a function of the iteration step for $J/B = 1$. Convergence is shown to occur to the global and local minimum respectively. Rotational invariance refers to the rotational symmetry of the system. Rotating the system, therefore relabelling the lattice points by means of cyclic permutation, will not lead to a different energy.

The magnet that is considered here does not contain just one single energy minimum in parameter space. For a special choice of parameters, it is possible that the SPSA algorithm guarantees convergence towards the local minimum rather than the desired global minimum. This is shown in 4.3.

The global minimum corresponds to a fully anti-ferromagnetic configuration. Each neighbouring spin is antiparallel along the z-axis. The local minimum, on the other hand, corresponds to a state where two sets of spins are anti-parallel to one another, while the spins within the sets are parallel to each other. While it is not energetically favourable within the entire parameter space, if the SPSA algorithm approaches the state close enough, it is possible that the algorithm can not update the parameters such that the global minimum is found any more because the remaining steps may be too small. Two of the states for each energy are given in figure 4.4.

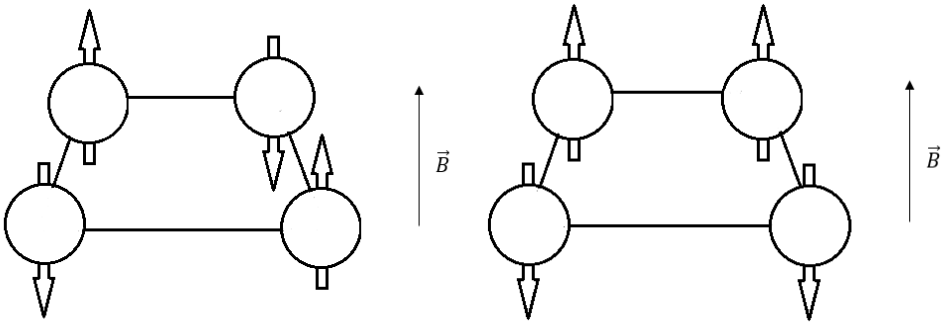

(a) Configuration of the global minimum.

(b) Configuration of the local minimum.

Figure 4.4: The configurations of the two energy minima for $J/B = 1$, where each spin is projected along the z-axis.

5 Conclusion and Discussion

5.1 Conclusion

The variational quantum eigensolver is a strong tool for the field of (quantum) chemistry and physics and will be one the very first successes in the field of quantum computing. A fully fledged universal quantum computer is still facing too many challenges to be realized within the next few years. Small quantum registers that are specialized for one certain task can already supersede classical computers in their respective field, though. In this thesis, it has been shown that a hybrid computer with at its core a quantum simulator running the variational quantum eigensolving algorithm can be utilized for the calculation of the potential curve of the hydrogen molecule. From this curve, the bonding length and molecular properties such as reaction rates can be deduced. The versatility of the VQE algorithm has been showcased by applying it to the problem of quantum magnetism as well. This new type of simulation can lead to a paradigm shift from a qualitative way of understanding physical phenomena to a quantitative one. This enables predictive power, one of the strongest powers belonging to the scientific method. This is very useful in fields like nuclear fusion as well, where exact answers are often desired, like the existence of resonance peaks.

Despite the fact that the bonding simulations match the exact Hartree-Fock curve, this is not the final product. The energy dip ΔE in the curve can be used for the calculation of molecular properties, some of which scale exponentially with this dip. A hard limit on the chemical accuracy has to be imposed to reduce the error in these chemical properties. The difference between the exact Hartree-Fock and the experimental values are, at most, of the same order as the absolute value of these energy values. This means that even if exact correspondence were to occur between the perfect simulations and the Hartree-Fock procedure, these answers would fall outside of the chemical accuracy regime of the actual experimental values and may therefore be rendered useless. Accounting for effects such as relativistic effects, rejecting the Born-Oppenheimer approximation, using non-spherical orbitals, employing a more accurate STO-nG basis and introducing spin-spin interactions will likely lead to a more accurate for the simulations themselves. Aiming for chemical accuracy is most useful and practical in the latter case, but it has been shown that it is possible to begin with for a simplified case.

For general simulations, sufficient entanglement is required for the circuit to accurately acquire the correct answer. The implementation of a multi-qubit entanglement operation would therefore be advantageous to the success of the hybrid computer. Real simulations on actual quantum computers must show how entanglement plays a role in the accuracy of the computation and what effects decoherence and quantum gate deficiencies have on the final results.

Finally, the SPSA might find local energy minima which may not always be of interest. The algorithm relies on a good initial state from which it starts looking for the ground energy. This good state may not always be known a priori, and such a state must be guessed. If it is unsure whether multiple minima exists, the algorithm can be run continuously.

5.2 The future of quantum computing

A hybrid computer combining the elements of both classical and quantum computation seems to have a very bright future. The final goal is to construct a universal quantum computer that exceeds classical computers in almost every aspect of computation. The hybrid computer may in fact pave the way for this new era of technology. Different algorithms have been shown to show quantum supremacy, such as simulations, Shor's algorithm and Grover's algorithm. Mankind is nowhere near the final version of the quantum computer, but serious advancements are being made every single day, both theoretically and in practice. The future of quantum computing is promising!

References

[1] P.W. Shor. Algorithms for quantum computation: discrete logarithms and factoring. *Foundations of Computer Science*, pages 124–134, 1994.

[2] E. Kassal, J.D. Whitfield, A. Perdomo-Ortiz, M. Yung, A. Aspuru-Guzik. Simulating Chemistry on a Quantum Computer. arXiv:1007.2648v1, 15 July 2010.

[3] B.P. Lanyon, J.D. Whitfield, G.G. Gillett, M.E. Goggin, M.P. Almeida, I. Kassal, J.D. Biamonte, M. Mohseni, B.J. Powell, M. Barbieri, A. Aspuru-Guzik, A.G. White. Towards quantum chemistry on a quantum computer. *Nature*, 2(2):106–111, 2010. doi: https://doi.org/10.1038/nchem.483.

[4] J.D. Whitfield, J. Biamonte, A. Aspuru-Guzik. Simulation of electronic structure hamiltonians using quantum computers. *Journal of Physics A: Mathematical and Theoretical*, 109(5):735–750, 2010. doi: https://doi.org/10.1080/00268976.2011.552441.

[5] A. Peruzzo, J. McClean, P. Shadbolt, M. Yung, X. Zhou, P.J. Love, A. Aspuru-Guzik, J.L. O'Brien. A variational eigenvalue solver on a photonic quantum processor. *Nature*, 5:4213, 2014.

[6] A. Kandala, A. Mezzacapo, K. Temme, M. Takita, M. Brink, J.M. Chow, J.M. Gambetta. Hardware-efficient variational quantum eigensolver for small molecules and quantum magnets. *Nature*, 549: 242–246, 2017. doi: https://doi.org/10.1103/PhysRevX.8.011021.

[7] Ed Pell. How to measure a molecule's energy using a quantum computer, 2017. URL `https://www.ibm.com/blogs/research/2017/09/quantum-molecule/`.

[8] P.J.J. O'Malley et al.

[9] R. Somma, G. Ortiz, J. E. Gubernatis, E. Knill, R. Laflamme. Simulating physical phenomena by quantum networks. *Phys. Rev. A*, 65(4):042323, 2002.

[10] J.C. Spall. An Overview of the Simultaneous Perturbation Method for Efficient Optimization. *Johns Hopkins APL Technical Digest*, 19(4):482–492, 1998.

[11] A. Kandala, A. Mezzacapo, K. Temme, M. Takita, M. Brink, J.M. Chow, J.M. Gambetta. Supplementary material for 'Hardware-efficient variational quantum eigensolver for small molecules and quantum magnets'. *Nature*, 549, 2017. doi: https://doi.org/10.1103/PhysRevX.8.011021.

[12] J.R. McClean, J. Romero, R. Babbush, A. Aspuru-Guzik. The theory of variational hybrid quantum-classical algorithms. *New Journal of Physics*, 18, 2016.

[13] S.B. Bravyi, A.Y. Kitaev,. Fermionic Quantum Computation. *Annals of Physics*, 298(1):210–226, 2002. doi: https://doi.org/10.1006/aphy.2002.6254.

[14] Matlab scripts available on request. j.j.postema@student.tue.nl, 2018.

[15] James Johns. Hartree Fock in Matlab, 2016. URL `https://www.youtube.com/channel/UCi_7bHjnsKbBx-VftBppLOQ`.

[16] niconeuman. Matlab-Hartree-Fock, 2018. URL `https://github.com/niconeuman/MATLAB-Hartree-Fock`.

[17] N. Moll. Private communication.

[18] R. Nave. Hydrogen Molecule. URL `http://hyperphysics.phy-astr.gsu.edu/hbase/molecule/hmol.html`.

[19] Moll, A. Fuhrer, P. Staar, I. Tavernelli N. Optimizing qubit resources for quantum chemistry simulations in second quantization on a quantum computer. *Journal of Physics A: Mathematical and Theoretical*, 49(29), 2016.

[20] E. Henögl, A. Pranter. H_2 bond potential with respect to the core distance. Student project, February 2014.

[21] J.I. Colless, V.V. Ramasesh, D. Dahlen, M.S. Blok, M.E. Kimchi-Schwartz, J.R. McClean, J. Carter, W.A. de Jong, I. Siddiqi. Computation of Molecular Spectra on a Quantum Processor with an Error-Resilient Algorithm. *Phys. Rev. X*, 8(1):011021, 2018.

Appendix A: A measurement protocol for Pauli products

In this Appendix, a protocol is given for the measurement of Pauli terms that is only valid for perfect simulations. A real quantum computer would operate using the same principles, but the distribution of qubit states is approximated by taking samples rather than being an a priori known distribution.

I. Single Pauli terms

If the Pauli term is $\mathbb{1}$, no measurement should take place. The coefficient in front of this term can be taken as a constant that is added up to the total.

If the Pauli term is Z, a single-qubit measurement should be performed. For perfect simulations, it is not a single measurement that is performed, such that the qubit collapses to either $|0\rangle$ or $|1\rangle$. Rather, the distribution of states is measured 'infinitely' and averaged. As an example, a Z-measurement is performed of the qubit state $|\phi\rangle = \alpha|0\rangle + \beta|1\rangle$. Because of the identification

$$Z|0\rangle = |0\rangle, Z|1\rangle = -|1\rangle, \tag{A.1}$$

the observation can be made that $\langle Z\rangle = \langle\phi|Z|\phi\rangle = \alpha - \beta$.

If the Pauli term is either X or Y, the sampling is straightforward up to a post-rotation.. Measurements take place in the Z-basis by definition. Measuring $\langle Z\rangle$ thus requires no post-rotation. A $\langle X\rangle$ measurement requires a $Y_{-\frac{\pi}{2}}$-rotation and a $\langle Y\rangle$-measurement requires a $X_{\frac{\pi}{2}}$-rotation. Afterwards, a regular measurement is performed.

II. Double Pauli terms

If both Pauli terms are $\mathbb{1}$, no measurement should take place. The coefficient in front of this term can be taken as a constant that is added up to the total.

If only one Pauli term is $\mathbb{1}$, only the remaining Pauli term must be measured according to protocol I.

If no Pauli term is $\mathbb{1}$, then the states of both qubits on which the Pauli terms are operating must be considered. As mathematical entities, their states are independent and the expectation values of Pauli terms are thus separable. In short,

$$\langle Z_1 Z_2\rangle = \langle Z\rangle_1 \langle Z\rangle_2, \tag{A.2}$$

such that symmetric states carry an eigenvalue of $+1$ and anti-symmetric states carry an eigenvalue of -1. Even if there exist entangled states, which are not independent single-qubit states, this procedure yields the correct result. If at least one of the two operators is not a Z-operator, post-rotations must be included to the respective qubits.

III. Multiple Pauli terms

If all Pauli terms are $\mathbb{1}$, no measurement should take place. The coefficient in front of this term can be taken as a constant that is added up to the total.

If only one or two Pauli terms are not $\mathbb{1}$, protocol I. or II. must be invoked.

If more than three Pauli terms are not $\mathbb{1}$, one can no longer look at the single states 'spin-up' and 'spin-down', but rather at combinatory states. The spin-parity of the system now describes the eigenvalue of the Z-operator instead of the single-spin configuration. The parity numbers $\pi = +1$ and $\pi = -1$ are assigned to the states $|0\rangle$ and $|1\rangle$ respectively. For quantum state that is expressed as the product of single-particle states, the parity as a whole is equal to the product of the single-particle parities. Implicitly, this formalism has been applied to protocol II. as well. For example, a Z-measurement of the qubit state $|\phi\rangle = \alpha|001\rangle + \beta|011\rangle$ yields the expectation value $\langle Z\rangle = \langle\phi|Z|\phi\rangle = -\alpha + \beta$. If appropriate, post-rotations must be applied to the respective qubits.

Appendix B: First quantization treatment of H_2

The hydrogen molecule can be treated in terms of spatial wave functions and spin functions, known as the first quantization formalism. Let A and B denote the first and second proton respectively, and let $\vec{r}_1$ and $\vec{r}_2$ denote the position vectors of the first and second electron respectively, relative to the nucleus their wave function index belongs to. Under the Born-Oppenheimer approximation, the wave function ansatz for both the bonding and anti-bonding can be stipulated as

$$\Psi = (\alpha_1\beta_2 - \beta_1\alpha_2)(\psi_A(\vec{r}_1)\psi_B(\vec{r}_2) + \psi_A(\vec{r}_2)\psi_B(\vec{r}_1)), \tag{A.3}$$

$$\Psi = (\alpha_1\alpha_2)(\psi_A(\vec{r}_1)\psi_B(\vec{r}_2) - \psi_A(\vec{r}_2)\psi_B(\vec{r}_1)), \tag{A.4}$$

such that the desired fermionic antisymmetry has been imposed on the wave function. Here, ψ_I denotes the spatial wave function of an electron around nucleus I.

The additional assumption is made that the electrons are located in $1s$ orbitals that do not deform under the presence of an additional hydrogen atom. Each electron can then be described by the spatial wave function

$$\psi_I(\vec{r}_j) = \frac{1}{\sqrt{\pi a_0^3}} e^{\frac{-|\vec{r}_j|}{a_0}}, \tag{A.5}$$

where a_0 denotes the Bohr radius.

The Hamiltonian of the system can written as

$$\mathcal{H} = \underbrace{-\frac{\hbar^2}{2m_p}(\Delta_A + \Delta_B)}_{\text{I.}} \underbrace{-\frac{\hbar^2}{2m_e}(\Delta_1 + \Delta_2)}_{\text{II.}} \underbrace{-\frac{e^2}{4\pi\epsilon_0}(\frac{1}{r_{A1}} + \frac{1}{r_{B2}})}_{\text{III.}} \underbrace{-\frac{e^2}{4\pi\epsilon_0}(\frac{1}{r_{A2}} + \frac{1}{r_{B1}} - \frac{1}{R} - \frac{1}{r_{12}})}_{\text{IV.}}, \tag{A.6}$$

where m_p is the mass of the proton, m_e the mass of an electron, Δ_I the Laplacian operator on proton I, Δ_j the Laplacian operator on electron j, e the elementary charge and ϵ_0 the vacuum permittivity. Furthermore, the distances are defined as follows: r_{Ij} is the distance between proton I and electron j, R is the distance between the two protons and r_{12} is the distance between the two electrons.

Under the Born-Oppenheimer approximation, $I.$ is omitted by definition. Parts $II.$ and $III.$ are the Hamiltonians of which the functions $\psi_A(\vec{r}_1)$ and $\psi_B(\vec{r}_2)$ are the eigenfunctions, with eigenvalue $E_0 = -13.6$ eV. The energy E of a certain given geometry is given by

$$E = \langle H \rangle = \frac{\iint \Psi\mathcal{H}\Psi \, dV_1 \, dV_2}{\iint \Psi\Psi \, dV_1 \, dV_2}, \tag{A.7}$$

where the $\iint \Psi\Psi \, dV_1 \, dV_2$ part has to be taken into account explicitly for non-normalized functions such as (A.3) and (A.4). For ease of notation, the conjugation has been omitted.

Due to certain symmetries in the system and the fact that the integrals contain the Hamiltonians of isolated hydrogen atoms as well as their eigenfunctions, $\iint \Psi\Psi \, dV_1 \, dV_2$ can be written as

$$2\iint [\psi_A(\vec{r}_1)^2\psi_B(\vec{r}_2)^2 + \psi_A(\vec{r}_1)\psi_A(\vec{r}_2)\psi_B(\vec{r}_1)\psi_B(\vec{r}_2)][2E_0 - \frac{e^2}{4\pi\epsilon_0}(\frac{1}{r_{A2}} + \frac{1}{r_{B1}} - \frac{1}{R} - \frac{1}{r_{12}})] \, dV_1 \, dV_2 \tag{A.8}$$

in which certain integrals can be recognized. These include [20]

1. The Coulomb integral

$$C \overset{\text{def}}{=} \int \psi_A(\vec{r}_1)^2(-\frac{e^2}{4\pi\epsilon_0 r_{B1}}) \, dV_1 \tag{A.9}$$

that describes the Coulomb attraction between an electron, in the $1s$ state around one proton, with the other proton. The integral is symmetric under the simultaneous exchange of protons and electrons.

2. The overlap integral

$$S \stackrel{\text{def}}{=} \int \psi_A(\vec{r}_1)\psi_B(\vec{r}_1)\, dV_1 \tag{A.10}$$

that describes the probability of an electron that is located exactly between the two nuclei to *not* belong to a certain nucleus. It is a measure of the degree of overlap of the integrals.

3. The one electron exchange integral

$$X \stackrel{\text{def}}{=} \int \psi_A(\vec{r}_1)\psi_B(\vec{r}_1)(-\frac{e^2}{4\pi\epsilon_0 r_{B1}})\, dV_1 \tag{A.11}$$

that describes an electron between the two nuclei interacting with a proton, specified by the integral.

4. The pure electronic Coulomb integral

$$P \stackrel{\text{def}}{=} \iint \psi_A(\vec{r}_1)^2\psi_B(\vec{r}_2)^2 \frac{e^2}{4\pi\epsilon_0 r_{12}}\, dV_1\, dV_2 \tag{A.12}$$

that describes the Coulomb interaction between two electrons that are purely in their $1s$ state around their respective nuclei.

5. The mixed electronic Coulomb integral

$$M \stackrel{\text{def}}{=} \iint \psi_A(\vec{r}_1)\psi_B(\vec{r}_1)\psi_A(\vec{r}_2)\psi_B(\vec{r}_2) \frac{e^2}{4\pi\epsilon_0 r_{12}}\, dV_1\, dV_2 \tag{A.13}$$

that describes the Coulomb interaction between electrons in mixed states, called the exchange density.

Finally, the bond potential may be written down as a function of these integrals as

$$E = 2E_0 + \frac{2C \pm 2XS + P + M}{1 \pm S^2} + \frac{e^2}{4\pi\epsilon_0 R}. \tag{A.14}$$

The electrostatic repulsion of the two protons has been taken into account separately, as this part of the integral (A.8) was not involved in the integrals C, S, X, P and M. Clearly, in the limit of infinite separation,

$$\lim_{R\to\infty} E = 2E_0$$

as expected for two isolated hydrogen atoms. The energy plots are shown in figure 5.1.

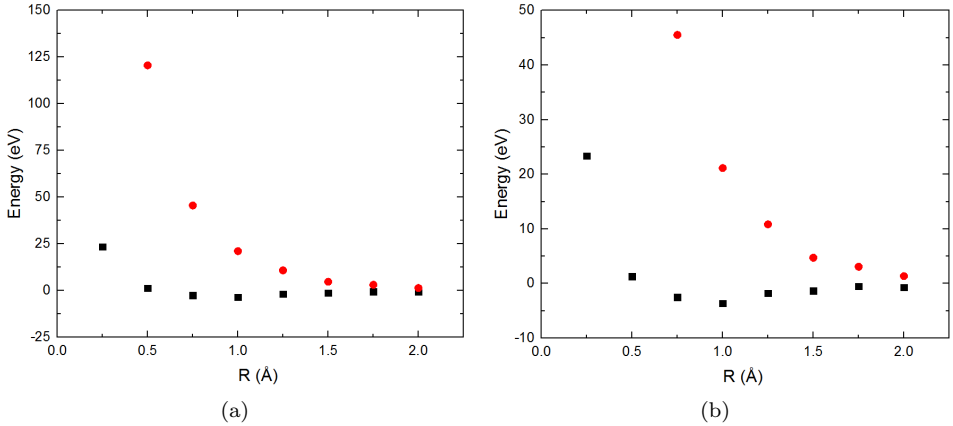

(a) (b)

Figure 5.1: The potential landscape for H_2 bonding (black squares) and anti-bonding (red circles) states calculated by numerical integration.

The figure clearly shows an equilibrium bonding length around R =0.87 Å with an energy dip of −3.18 eV. Compared to the experimental values of R =0.7414 Å with an energy dip of −4.52 eV [18], the

simulations are off. This can be explained by two reasons. First, the wave functions deform under the presence of other atoms, yet they have been assumed to be spherical. Secondly, the integral bounds have been taken from -5 Å to 5 Å for ease of computation. Another result from the numerical integration is the seeming absence of smoothness around R =1.25 Å.

Despite these deviations and approximations, the general shape of the curve shows close agreement to experimental observations and an equilibrium bonding state can be made out.

Appendix C: Reduction scheme for the H_2 Hamiltonian

After applying the Jordan Wigner transformation (3.11) and (3.12) to the electronic Hamiltonian (3.5), one obtains the four-qubit hydrogen Hamiltonian

$$\hat{\mathcal{H}}^4 = f_1 + f_2 Z_1 Z_2 + f_2 Z_3 Z_4 + f_3 Z_1 Z_3 + f_3 Z_2 Z_4 + f_4 Z_2 Z_3 + f_5 Z_1 Z_4 + f_6 X_1 X_2 X_3 X_4 + f_6 X_1 X_2 Y_3 Y_4 + f_6 Y_1 Y_2 X_3 X_4 + f_6 Y_1 Y_2 Y_3 Y_4 + f_7 Z_1 + f_7 Z_4 + f_8 Z_2 + f_8 Z_3, \quad \text{(A.15)}$$

which can be put in matrix form

$$\hat{\mathcal{H}}^4 = \begin{pmatrix} A & 0 & 0 & 0 & 0 & 0 & 0 & 0 & 0 & 0 & 0 & 0 & 0 & 0 & 0 & 0 \\ 0 & B & 0 & 0 & 0 & 0 & 0 & 0 & 0 & 0 & 0 & 0 & 0 & 0 & 0 & 0 \\ 0 & 0 & C & 0 & 0 & 0 & 0 & 0 & 0 & 0 & 0 & 0 & 0 & 0 & 0 & 0 \\ 0 & 0 & 0 & D & 0 & 0 & 0 & 0 & 0 & 0 & 0 & 0 & 0 & 0 & 0 & 0 \\ 0 & 0 & 0 & 0 & C & 0 & 0 & 0 & 0 & 0 & 0 & 0 & 0 & 0 & 0 & 0 \\ 0 & 0 & 0 & 0 & 0 & E & 0 & 0 & 0 & 0 & 4f_6 & 0 & 0 & 0 & 0 & 0 \\ 0 & 0 & 0 & 0 & 0 & 0 & F & 0 & 0 & 4f_6 & 0 & 0 & 0 & 0 & 0 & 0 \\ 0 & 0 & 0 & 0 & 0 & 0 & 0 & G & 0 & 0 & 0 & 0 & 0 & 0 & 0 & 0 \\ 0 & 0 & 0 & 0 & 0 & 0 & 0 & 0 & B & 0 & 0 & 0 & 0 & 0 & 0 & 0 \\ 0 & 0 & 0 & 0 & 0 & 0 & 4f_6 & 0 & 0 & H & 0 & 0 & 0 & 0 & 0 & 0 \\ 0 & 0 & 0 & 0 & 0 & 4f_6 & 0 & 0 & 0 & 0 & E & 0 & 0 & 0 & 0 & 0 \\ 0 & 0 & 0 & 0 & 0 & 0 & 0 & 0 & 0 & 0 & 0 & I & 0 & 0 & 0 & 0 \\ 0 & 0 & 0 & 0 & 0 & 0 & 0 & 0 & 0 & 0 & 0 & 0 & D & 0 & 0 & 0 \\ 0 & 0 & 0 & 0 & 0 & 0 & 0 & 0 & 0 & 0 & 0 & 0 & 0 & I & 0 & 0 \\ 0 & 0 & 0 & 0 & 0 & 0 & 0 & 0 & 0 & 0 & 0 & 0 & 0 & 0 & G & 0 \\ 0 & 0 & 0 & 0 & 0 & 0 & 0 & 0 & 0 & 0 & 0 & 0 & 0 & 0 & 0 & J \end{pmatrix}, \quad \text{(A.16)}$$

where the letters are functions of the f-coefficients according to

$$A = f_1 + 2f_2 + 2f_3 + f_4 + f_5 + 2f_7 + 2f_8,$$

$$B = f_1 + f_4 - f_5 + 2f_8,$$

$$C = f_1 - 2f_4 + f_5 + 2f_7 + 2f_7,$$

$$D = f_1 + 2f_2 - 2f_3 - f_4 - f_5,$$

$$E = f_1 - 2f_2 + 2f_3 - f_4 - f_5,$$

$$F = f_1 - 2f_2 - 2f_3 + f_4 + f_5 + 2f_7 - 2f_8,$$

$$G = f_1 + f_4 - f_5 - 2f_8,$$

$$H = f_1 - 2f_2 - 2f_3 + f_4 + f_5 - 2f_7 + 2f_8,$$

$$I = f_1 - f_4 + f_5 - 2f_7,$$

$$J = f_1 + 2f_2 + 2f_3 + f_4 + f_5 - 2f_7 - 2f_8.$$

The f-coefficients are functions of the integrals (3.9) and (3.10):

$$f_1 = h_{11} - \frac{h_{1212}}{2} + h_{1221} + \frac{h_{1441}}{4} + h_{22} + \frac{h_{2332}}{4},$$

$$f_2 = \frac{h_{1221}}{4} - \frac{h_{1212}}{4},$$

$$f_3 = \frac{h_{1221}}{4},$$

$$f_4 = \frac{h_{2332}}{4},$$

$$f_5 = \frac{h_{1441}}{4},$$

$$f_6 = \frac{h_{1212}}{4},$$

$$f_7 = -\frac{h_{11}}{2} + \frac{h_{1212}}{4} - \frac{h_{1221}}{2} - \frac{h_{1441}}{4},$$

$$f_8 = \frac{h_{1212}}{4} - \frac{h_{1221}}{2} - \frac{h_{22}}{2} - \frac{h_{2332}}{4}.$$

The only block that is of interest for molecular bonding is the block describing 2 electrons in the singlet state. The Hamiltonian $\hat{\mathcal{H}}^4_{sparse}$describing this state is equal to $\hat{\mathcal{H}}^4_{sparse} = {\Pi^4_2}^\dagger\, \hat{\mathcal{H}}\, \Pi^4_2$, where Π^4_2 is given by equation (3.16). The new Hamiltonian looks like

$$\hat{\mathcal{H}}^4_{sparse} = \begin{pmatrix} 0&0&0&0&0&0&0&0&0&0&0&0&0&0&0&0 \\ 0&0&0&0&0&0&0&0&0&0&0&0&0&0&0&0 \\ 0&0&0&0&0&0&0&0&0&0&0&0&0&0&0&0 \\ 0&0&0&0&0&0&0&0&0&0&0&0&0&0&0&0 \\ 0&0&0&0&0&0&0&0&0&0&0&0&0&0&0&0 \\ 0&0&0&0&0&E&0&0&0&0&4f_6&0&0&0&0&0 \\ 0&0&0&0&0&0&F&0&0&4f_6&0&0&0&0&0&0 \\ 0&0&0&0&0&0&0&0&0&0&0&0&0&0&0&0 \\ 0&0&0&0&0&0&0&0&0&0&0&0&0&0&0&0 \\ 0&0&0&0&0&0&4f_6&0&0&H&0&0&0&0&0&0 \\ 0&0&0&0&0&4f_6&0&0&0&0&E&0&0&0&0&0 \\ 0&0&0&0&0&0&0&0&0&0&0&0&0&0&0&0 \\ 0&0&0&0&0&0&0&0&0&0&0&0&0&0&0&0 \\ 0&0&0&0&0&0&0&0&0&0&0&0&0&0&0&0 \\ 0&0&0&0&0&0&0&0&0&0&0&0&0&0&0&0 \\ 0&0&0&0&0&0&0&0&0&0&0&0&0&0&0&0 \end{pmatrix}. \tag{A.17}$$

The inner 8×8 block can be taken out of the Hamiltonian. This can be achieved formally by applying shift operators to the matrix, but this is not necessary. One obtains the 3-qubit Hamiltonian

$$\hat{\mathcal{H}}^3 = \begin{pmatrix} 0&0&0&0&0&0&0&0 \\ 0&E&0&0&0&0&4f_6&0 \\ 0&0&F&0&0&4f_6&0&0 \\ 0&0&0&0&0&0&0&0 \\ 0&0&0&0&0&0&0&0 \\ 0&0&4f_6&0&0&H&0&0 \\ 0&4f_6&0&0&0&0&E&0 \\ 0&0&0&0&0&0&0&0 \end{pmatrix}. \tag{A.18}$$

This matrix can be re-ordered such that it contains an inner 4×4 block such that the dimensionality can be reduced from 3 qubits to 2. Let the 3-dimensional reorder operator be given by

$$R = \frac{1}{2}(1 + Z_1Z_3 - Z_1X_2Z_3 + X_2). \tag{A.19}$$

The reordered Hamiltonian is now given by

$$\hat{\mathcal{H}}^3_{order} = R^\dagger \hat{\mathcal{H}}^3 R = \begin{pmatrix} 0&0&0&0&0&0&0&0 \\ 0&0&0&0&0&0&0&0 \\ 0&0&F&0&0&4f_6&0&0 \\ 0&0&0&E&4f_6&0&0&0 \\ 0&0&0&4f_6&E&0&0&0 \\ 0&0&4f_6&0&0&H&0&0 \\ 0&0&0&0&0&0&0&0 \\ 0&0&0&0&0&0&0&0 \end{pmatrix}. \tag{A.20}$$

The final 2-qubit Hamiltonian equals

$$\hat{\mathcal{H}}^2 = \begin{pmatrix} F & 0 & 0 & 4f_6 \\ 0 & E & 4f_6 & 0 \\ 0 & 4f_6 & E & 0 \\ 4f_6 & 0 & 0 & H \end{pmatrix}. \tag{A.21}$$

The identification

$$g_0 = f_1 - 2f_2,\ g_1 = f_7 - f_8,\ g_2 = 4f_6,\ g_3 = -2f_3 + f_4 + f_5$$

gives the final result (3.18).

Appendix D: Table of H_2 Hamiltonian terms

Table 1: The coefficients of the hydrogen Hamiltonian (3.18) in Hartrees as a function of the inter-nuclear distance R (in Å) [21]. The electrostatic proton-proton repulsion is implicitly added on the diagonal.

R	**g0 (II)**	**g1 (IZ/ZI)**	**g2 (XX)**	**g3 (ZZ)**
0.05	1.00777E+01	-1.05533E+00	1.55708E-01	1.39333E-02
0.10	4.75665E+00	-1.02731E+00	1.56170E-01	1.38667E-02
0.15	2.94817E+00	-9.84234E-01	1.56930E-01	1.37610E-02
0.20	2.01153E+00	-9.30489E-01	1.57973E-01	1.36238E-02
0.25	1.42283E+00	-8.70646E-01	1.59277E-01	1.34635E-02
0.30	1.01018E+00	-8.08649E-01	1.60818E-01	1.32880E-02
0.35	7.01273E-01	-7.47416E-01	1.62573E-01	1.31036E-02
0.40	4.60364E-01	-6.88819E-01	1.64515E-01	1.29140E-02
0.45	2.67547E-01	-6.33890E-01	1.66621E-01	1.27192E-02
0.50	1.10647E-01	-5.83080E-01	1.68870E-01	1.25165E-02
0.55	-1.83734E-02	-5.36489E-01	1.71244E-01	1.23003E-02
0.65	-2.13932E-01	-4.55433E-01	1.76318E-01	1.18019E-02
0.75	-3.49833E-01	-3.88748E-01	1.81771E-01	1.11772E-02
0.85	-4.45424E-01	-3.33747E-01	1.87562E-01	1.04061E-02
0.95	-5.13548E-01	-2.87796E-01	1.93650E-01	9.50345E-03
1.05	-5.62600E-01	-2.48783E-01	1.99984E-01	8.50998E-03
1.15	-5.97973E-01	-2.15234E-01	2.06495E-01	7.47722E-03
1.25	-6.23223E-01	-1.86173E-01	2.13102E-01	6.45563E-03
1.35	-6.40837E-01	-1.60926E-01	2.19727E-01	5.48623E-03
1.45	-6.52661E-01	-1.38977E-01	2.26294E-01	4.59760E-03
1.55	-6.60117E-01	-1.19894E-01	2.32740E-01	3.80558E-03
1.65	-6.64309E-01	-1.03305E-01	2.39014E-01	3.11545E-03
1.75	-6.66092E-01	-8.88906E-02	2.45075E-01	2.52480E-03
1.85	-6.66126E-01	-7.63712E-02	2.50896E-01	2.02647E-03
1.95	-6.64916E-01	-6.55065E-02	2.56458E-01	1.61100E-03
2.05	-6.62844E-01	-5.60866E-02	2.61750E-01	1.26812E-03
2.15	-6.60199E-01	-4.79275E-02	2.66768E-01	9.88000E-04
2.25	-6.57196E-01	-4.08672E-02	2.71512E-01	7.61425E-04
2.35	-6.53992E-01	-3.47636E-02	2.75986E-01	5.80225E-04
2.45	-6.50702E-01	-2.94924E-02	2.80199E-01	4.36875E-04
2.55	-6.47408E-01	-2.49459E-02	2.84160E-01	3.25025E-04
2.65	-6.44165E-01	-2.10309E-02	2.87881E-01	2.38800E-04
2.75	-6.41011E-01	-1.76672E-02	2.91376E-01	1.73300E-04
2.85	-6.37971E-01	-1.47853E-02	2.94658E-01	1.24200E-04
2.95	-6.35058E-01	-1.23246E-02	2.97741E-01	8.78750E-05
3.05	-6.32279E-01	-1.02318E-02	3.00638E-01	6.14500E-05
3.15	-6.29635E-01	-8.45958E-03	3.03362E-01	4.24250E-05
3.25	-6.27126E-01	-6.96585E-03	3.05927E-01	2.89500E-05
3.35	-6.24746E-01	-5.71280E-03	3.08344E-01	1.95500E-05
3.45	-6.22491E-01	-4.66670E-03	3.10625E-01	1.30500E-05
3.55	-6.20353E-01	-3.79743E-03	3.12780E-01	8.57500E-06
3.65	-6.18325E-01	-3.07840E-03	3.14819E-01	5.60000E-06
3.75	-6.16401E-01	-2.48625E-03	3.16750E-01	3.60000E-06
3.85	-6.14575E-01	-2.00063E-03	3.18581E-01	2.27500E-06
3.95	-6.12839E-01	-1.60393E-03	3.20320E-01	1.42500E-06